applied sciences

MDPI

Article

An Investigation of Parameter Dimension Reduction Optimization of PMA-Synrm

Zhongqi Liu [1,*], Guiyuan Zhang [2] and Guanghui Du [2]

[1] School of Electrical Engineering, Zhejiang University of Water Resources and Electric Power, Hangzhou 310018, China
[2] School of Electrical and Control Engineering, Xi'an University of Science and Technology, Xi'an 710054, China; gyzhang2023@163.com (G.Z.); duguanghui1104@163.com (G.D.)
* Correspondence: liuzhongqi920@163.com

Abstract: The rotor of a permanent magnet-assisted synchronous reluctance (PMA-Synrm) motor mostly adopts the structure of a multi-layer magnetic barrier and multi-layer ferrite, which leads to the design parameters of this kind of motor increase with the increase in the number of magnetic barrier layers. A large number of design parameters are coupled with each other, which makes the optimization design of a permanent magnet-assisted synchronous reluctance motor particularly difficult. In this paper, a 7.5 kW, 1500 rpm permanent magnet-assisted synchronous reluctance motor is taken as the research object, and the optimization design of parameter dimension reduction is studied. The rotor structure of the motor is a combination of five layers of magnetic barrier and five layers of ferrite. By using the parameter dimension reduction method proposed in this paper, the number of parameters involved in the optimization is reduced from 26 to 7, which greatly improves the optimization efficiency of this kind of motor and realizes the comprehensive global optimization design of a permanent magnet-assisted synchronous reluctance motor. This paper provides a reference for the optimization of a permanent magnet-assisted synchronous reluctance motor.

Keywords: permanent magnet-assisted synchronous reluctance motor; electromagnetic property; temperature; finite element analysis; optimal design

Academic Editor: Pedro Couto

Received: 13 January 2025
Revised: 27 January 2025
Accepted: 31 January 2025
Published: 3 February 2025

Citation: Liu, Z.; Zhang, G.; Du, G. An Investigation of Parameter Dimension Reduction Optimization of PMA-Synrm. *Appl. Sci.* **2025**, *15*, 1529. https://doi.org/10.3390/app15031529

1. Introduction

A permanent magnet-assisted synchronous reluctance motor combines the characteristics of a synchronous reluctance motor and a permanent magnet synchronous motor [1]. It has higher power density and a wider speed range, and the performance of motor power factor and efficiency is second only to permanent magnet synchronous motor [2,3]. However, the manufacturing cost of a permanent magnet-assisted reluctance motor is much lower than that of a permanent magnet synchronous motor [4,5] because it only uses ferrite to assist magnetism. Therefore, a permanent magnet-assisted synchronous reluctance motor has become an important research object for the development of motor to "no rare earth, less rare earth". At present, a permanent magnet-assisted synchronous reluctance motor has become a research hotspot and has been applied in household appliances, low-voltage industry, electric vehicles, and low-speed high-torque fields.

At present, the research on a permanent magnet-assisted synchronous reluctance motor is mainly aimed at the analysis and design of rotor structure and the optimization design of the motor. In terms of rotor structure, the effects of the number of rotor magnetic barrier layers, the position and shape of the rotor magnetic barrier, and the proportion of rotor

magnetic barrier on the main performance of a permanent magnet-assisted synchronous reluctance motor are studied. The basic design rules of a permanent magnet-assisted synchronous reluctance motor are summarized [6]. In [7,8], the influence of different magnetic saturation degrees on the performance of a synchronous reluctance motor is studied. In addition, the electromagnetic performance of the synchronous reluctance motor before and after inserting the permanent magnet is compared and analyzed. The anti-demagnetization research of a permanent magnet-assisted synchronous reluctance motor is also a hot spot. Refs. [9,10] proposed a new rotor structure. Several bypass ribs are opened in the rotor magnetic barrier to provide a path for the demagnetization of the armature winding. Finally, the effect of reducing the output torque ripple of the motor and improving the anti-demagnetization ability of the motor is achieved. There are also many studies on ferrite design in a permanent magnet-assisted synchronous reluctance motor. These studies mainly focus on the influence of permanent magnet placement position, permanent magnet layer number, and permanent magnet insertion position on the electromagnetic performance of a permanent magnet-assisted synchronous reluctance motor [11,12]. In addition, many scholars have adopted an asymmetric rotor structure to improve the performance of a permanent magnet-assisted synchronous reluctance motor [13,14]. In general, the current research on the rotor structure of a permanent magnet-assisted synchronous reluctance motor is more detailed, which has great guiding significance for the design of such motors.

The research on the optimization design of a permanent magnet-assisted synchronous reluctance motor is also gradually deepened. Ref. [15] proposed to optimize the permanent magnet-assisted synchronous reluctance motor by establishing a simplified analytical model. The analytical model can quickly calculate the optimal end angle of the magnetic isolation bridge to achieve the purpose of reducing the torque ripple of the motor. However, only the influence of the end angle of the magnetic bridge on the output torque ripple is considered. As shown in ref. [16], through a series of mathematical formulas commonly used in motors, the calculation formula of output torque is derived, and various parameters affecting the calculation formula of torque are constrained. Then, the torque of the synchronous reluctance motor is maximized by a genetic algorithm considering a set of mechanical, thermal, and efficiency constraints. In the optimization process, the selected optimization parameters do not involve the structural design parameters of the synchronous reluctance motor rotor. Ref. [17] optimized the design of a switched reluctance motor. The optimization parameters include motor body design parameters and motor control system parameters. According to the sensitivity of the parameters, the 10 optimization parameters are divided into three layers, and the multi-objective genetic algorithm is used for hierarchical optimization design. Ref. [18] proposed that the multi-objective genetic algorithm is used to optimize the design parameters of seven stator and rotor structures of a three-layer magnetic barrier permanent magnet-assisted synchronous reluctance motor. In the selection of optimization parameters, only some parameters that are considered to have a greater impact are selected, and the full-parameter influence of the permanent magnet-assisted synchronous reluctance motor is not considered. Refs. [19,20] shows that the optimization design of an asynchronous starting synchronous reluctance motor adopts the optimization method of the response surface. There are only three optimization parameters selected in this paper, and there is no clear explanation for the selection of optimization parameters. Only a few optimization parameters can achieve the optimization design when considering all the parameters. Ref. [21] optimizes the design of a three-layer magnetic barrier permanent magnet-assisted synchronous reluctance motor. Among them, the multi-objective genetic algorithm is used to optimize the rotor magnetic barrier of the permanent magnet-assisted synchronous reluctance motor. The nine magnetic barrier design parameters are divided into three levels according to the parameter sensitivity to

optimize them respectively. The influence of parameters such as magnetic barrier thickness, permanent magnet length, and magnetic barrier bridge thickness is not considered in the selection of optimization parameters [22]. The multi-objective genetic algorithm is used to optimize the design of a permanent magnet-assisted synchronous reluctance motor with three-layer magnetic barriers, mainly to optimize the design parameters of magnetic barriers and permanent magnets. Eleven design parameters were selected for optimization, and the influence of magnetic bridge thickness was missing in the selection of optimization parameters. In addition, 11 optimization parameters will make the optimization process cumbersome and lengthy.

It can be known from the above literature that the current research on the optimization design of a permanent magnet-assisted synchronous reluctance motor is mainly the exploration of optimization algorithms, and the optimization parameters selected in this literature are only a few, which is incomplete. The rotor design parameters of a permanent magnet-assisted synchronous reluctance motor are very many, and the parameters are coupled with each other, which jointly affect the performance of the motor. Therefore, it is not enough to select only a few parameters when optimizing the permanent magnet-assisted synchronous reluctance motor. The optimization of a permanent magnet-assisted synchronous reluctance motor should take into account comprehensiveness and globality. In this paper, the influence of rotor design parameters of a permanent magnet-assisted synchronous reluctance motor on the main performance of the motor is considered, and a parameter dimension reduction optimization method is provided. The optimization parameters are effectively reduced from 26 to 7, and the comprehensive global optimization of a permanent magnet-assisted synchronous reluctance motor is realized.

In this paper, based on a 7.5 kW, 1500 rpm permanent magnet-assisted synchronous reluctance motor, the research on parameter dimension reduction optimization is carried out. In Section 2, the performance index of the permanent magnet-assisted synchronous reluctance motor and the initial design scheme and performance data of the motor are proposed. Section 3 mainly describes the process of the parameter dimension reduction optimization method and the optimization design of a permanent magnet-assisted synchronous reluctance motor using this method. The experimental test of the prototype is in Section 4. The summary of the full text is in Section 5. The work shown in this paper provides a certain reference significance for the optimization design of a permanent magnet-assisted synchronous reluctance motor.

2. Motor Performance Index and Initial Design Scheme

2.1. Performance Index of a Permanent Magnet-Assisted Synchronous Reluctance Motor

In this paper, a 7.5 kW, 1500 rpm permanent magnet-assisted synchronous reluctance motor is studied. The performance index of the motor is shown in Table 1. The proposed performance index is standard IE5 energy efficiency level, which is of great significance for the research of a permanent magnet-assisted synchronous reluctance motor.

Table 1. Performance index of permanent magnet-assisted synchronous reluctance motor.

Parameter Name	Value
Rated power (kW)	7.5
Rated speed (rpm)	1500
Rated voltage (V)	380
Rated torque (Nm)	47.8
Power factor	$\geq$0.9
Efficiency (%)	$\geq$94
Torque ripple (%)	$\leq$5

2.2. Initial Design Scheme of Permanent Magnet-Assisted Synchronous Reluctance Motor

Figure 1 shows the cross-sectional view of the initial design scheme of the permanent magnet-assisted synchronous reluctance motor. It can be seen from the diagram that the rotor of the motor is composed of five layers of magnetic barrier and five layers of ferrite.

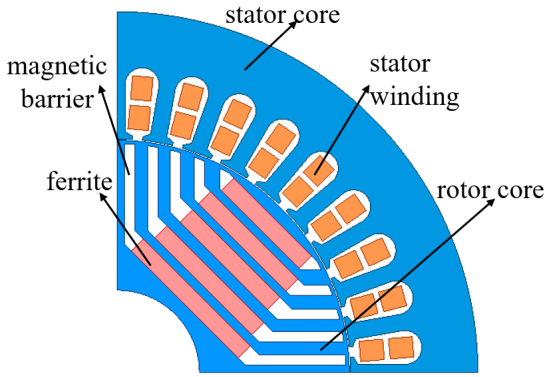

Figure 1. The 1/4 cross-section of the initial design scheme of permanent magnet-assisted synchronous reluctance motor.

Table 2 shows the basic design parameters and some electromagnetic properties of the initial design scheme. In the initial design of a permanent magnet-assisted synchronous reluctance motor, the basic size parameters of the motor can refer to the same power asynchronous motor. The finite element analysis of the initial design scheme shows that the torque ripple of the motor is as high as 15.6%, which does not meet the design requirements, and further optimization of the design of the motor is needed.

Table 2. The basic design parameters and performance of the initial design scheme.

Parameter Name	Value
Stator slot	36
Rotor pole	4
Stator outer diameter (mm)	210
Rotor outer diameter (mm)	135.2
Stack length (mm)	180
Airgap length (mm)	0.4
Iron core material	50BW600
Ferrite material	Y30
No-load back EMF (V)	85
Torque ripple (%)	15.6
Efficiency (%)	93.5
Power factor	0.92

3. Parameter Dimension Reduction Optimization Design of the PMA-Synrm

The permanent magnet-assisted synchronous reluctance motor studied in this paper is a rotor composed of five layers of magnetic barriers and five layers of ferrite, and the rotor design parameters are as high as 26. As shown in Figure 2, all the rotor design parameters of the motor are clearly marked. Table 3 mainly explains the rotor design parameters of a permanent magnet-assisted synchronous reluctance motor.

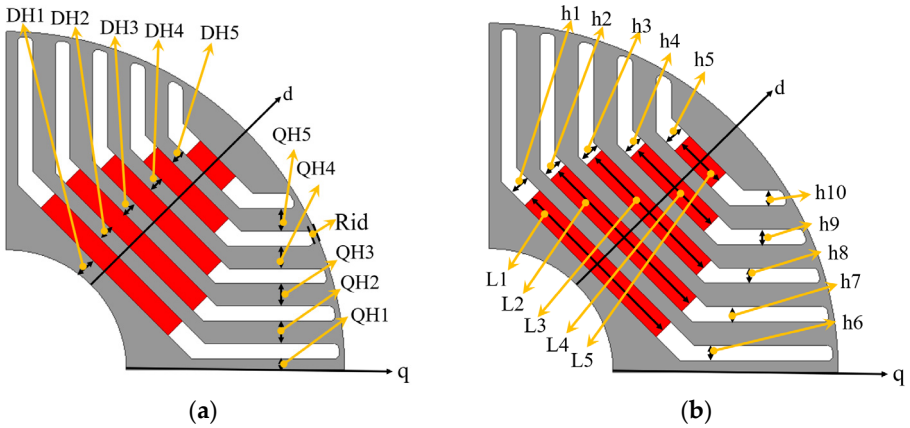

Figure 2. Design parameter diagram of permanent magnet-assisted synchronous reluctance motor rotor. (**a**) DH1–DH5, QH1–QH5 and Rid. (**b**) h1–h5, h6–h10 and L1–L5.

Table 3. Interpretation of rotor design parameters of permanent magnet-assisted synchronous reluctance motor.

Symbol	Meaning of Parameter
DH1-DH5	Thickness of d-axis five-layer magnetic layer
QH1-QH6	Thickness of q-axis five-layer magnetic layer
h1-h5	Thickness of d-axis five-layer magnetic barrier
h6-h10	Thickness of q-axis five-layer magnetic barrier
L1-L5	Length of five-layer ferrite
Rid	Length of circumferential magnetic bridge

3.1. Exploration of Parameter Dimension Reduction Optimization Method

It can be seen from the previous section that the rotor of the motor has 26 design parameters, and these design parameters are mutually coupled and influenced by each other, which is very unfavorable for the optimal design of the permanent magnet-assisted synchronous reluctance motor. Therefore, this section explores the parameter dimension reduction optimization method.

Figure 3 shows the influence of d-axis five-layer magnetic layer thickness (DH1–DH5), d-axis five-layer magnetic barrier thickness (h1–h5), q-axis five-layer magnetic layer thickness (QH1–QH5), and q-axis five-layer magnetic barrier thickness (h6–h10) on the output torque of the motor. It can be seen from the figure that the influence of each design parameter on the torque is not the same, but the change in the output torque is not more than 1.5 Nm, so the influence of these 20 design parameters on the output torque is small.

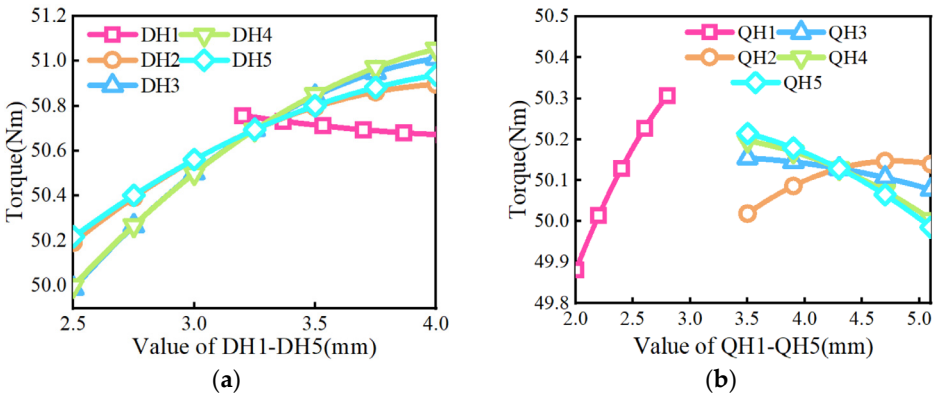

Figure 3. *Cont.*

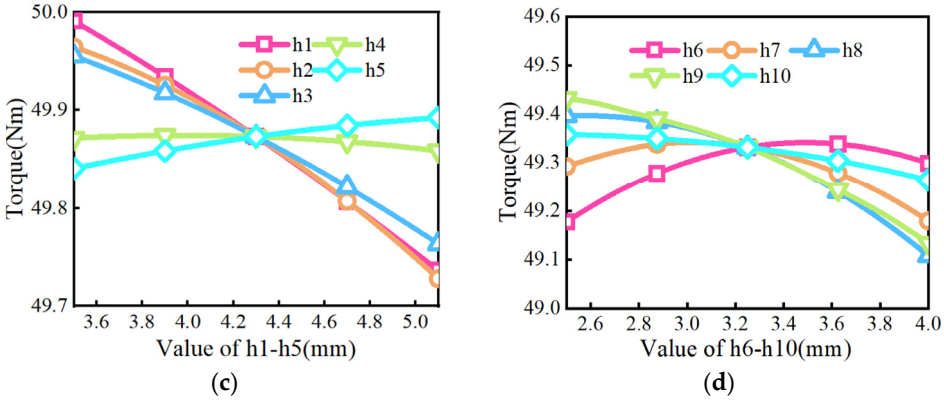

Figure 3. The influence of rotor design parameters on the output torque. (**a**) DH1–DH5. (**b**) QH1–QH5. (**c**) h1–h5. (**d**) h6–h10.

Based on the above analysis, two motors are designed, as shown in Figure 4. Figure 4a shows the motor models with different values of DH1–DH5, QH1–QH5, h1–h5, and h6–h10. Figure 4b shows the motor models with equal DH1–DH5, equal QH1–QH5, equal h1–h5, and equal h6–h10.

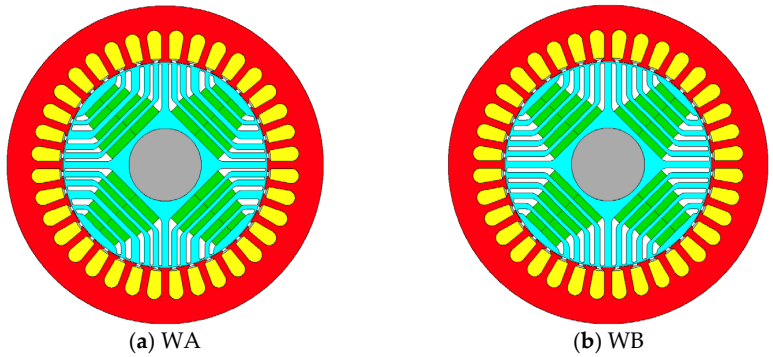

Figure 4. Cross-sectional view of two motors. (**a**) The values of DH1–DH5, QH1–QH5, h1–h5, and h6–h10 are different. (**b**) DH1–DH5 equal, QH1QH5 equal, h1–h5 equal, and h6–h10 equal.

The above two motors are excited by the same current source, and the calculation results are shown in Figure 5. It can be seen that the output torque of the motor with the same thickness (WA) is only 0.2 Nm different from that of the motor with different thicknesses (WB), but the torque ripple of the motor with the same thickness (WA) is only 10.6%, which is 9.5% lower than that of the motor with different thicknesses (WB). In addition, the difference in the rotor saliency ratio between the two motors is only 0.05.

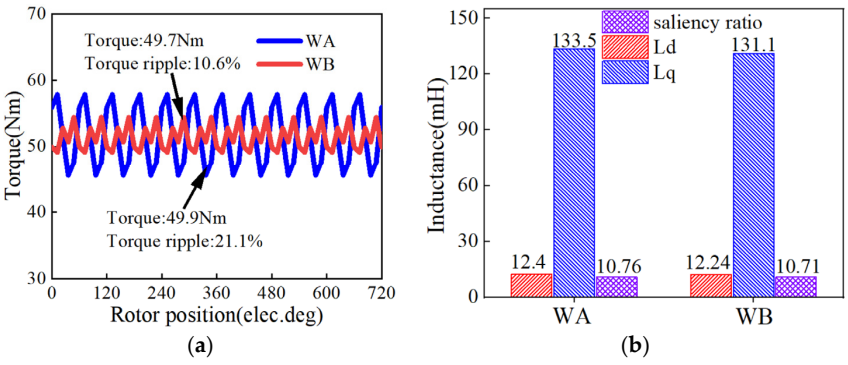

Figure 5. The torque characteristics and inductance characteristics of the two motors. (**a**) Torque characteristic. (**b**) Inductance characteristics.

According to the analysis of the influence of DH1-DH5, QH1-QH5, h1-h5, and h6-h10 on the output torque and the finite element analysis results of the above two motors, the hypothesis and the realization process of the parameter dimension reduction optimization design of the permanent magnet-assisted synchronous reluctance motor can be proposed, as shown in Figure 6.

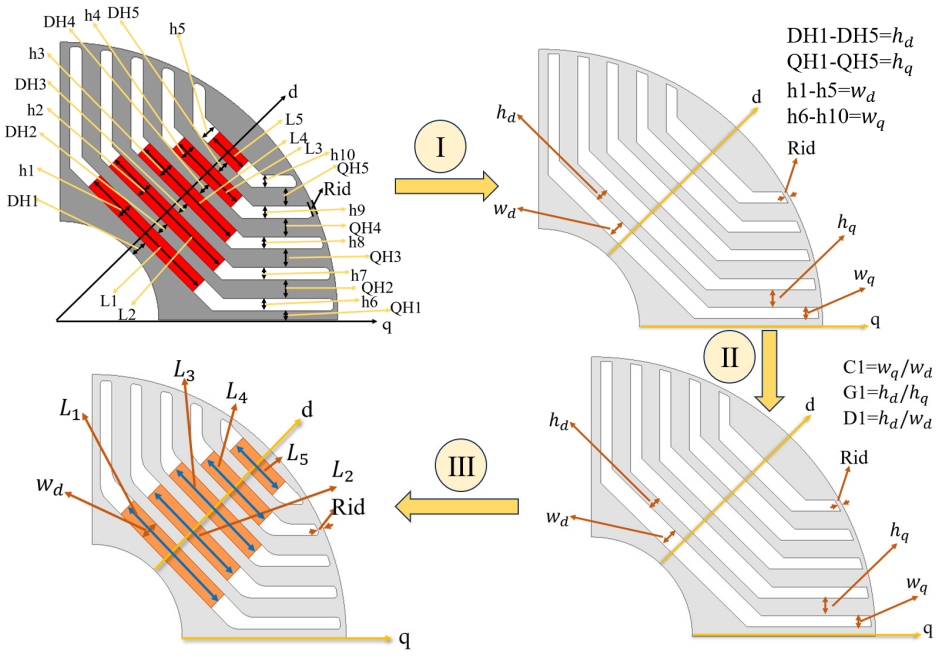

Figure 6. Parameter dimension reduction optimization flow chart.

Step 1: Assume that the thickness of the five magnetic barriers of the D axis is equal to w_d; it is assumed that the thickness of the magnetic layer between the magnetic barriers on the D axis is equal to h_d; suppose that the thickness of the five layers of the Q-axis magnetic barrier is equal to w_q; suppose that the thickness of the magnetic layer between the magnetic barriers on the Q axis is equal to h_q;

Step 2: Define C1, G1, D1, where C1 = w_q/w_d; G1 = h_d/h_q; D1 = h_d/w_d. Then, w_q, h_d, and h_q can be expressed by w_d. The optimal values of C1, G1, and D1 are obtained by optimizing the synchronous reluctance motor;

Step 3: Combined with the optimized C1, G1, D1, and w_d, other magnetic barrier parameters can be expressed. The final parameters of the permanent magnet-assisted synchronous reluctance motor are only w_d, L1–L5, and Rid.

3.2. Multi-Objective Optimization Design of Synrm

Figure 7 shows the synchronous reluctance motor model. From the diagram, it can be seen that after the hypothesis and the exploration of the relationship between the parameters, the design parameters of the synchronous reluctance motor are only w_d, C1, G1, D1, and Rid. Considering the processing technology, the Rid is constant at 1 mm.

Figure 8 shows the effects of G1, D1, and G1 on the electromagnetic performance of the motor. From Figure 8a, it can be seen that with the increase in C1, the output torque of the motor decreases continuously; with the increases in G1 and D1, the output torque of the motor also increases. Among them, G1 has the greatest influence on the output torque of the motor, and the variation range reaches 4.5 Nm. In Figure 8b, with the increases in C1 and D1, the torque ripple of the motor increases continuously, and the increase is close to 10%. However, with the increase in G1, the torque ripple of the motor decreases first and then increases, with a minimum of only 7% and a maximum of 33%. Therefore, G1

has the greatest influence on the torque ripple of the motor. From Figure 8c, it can be seen that with the increases in C1 and D1, the power factor of the motor changes little; with the increase in G1, the power factor of the motor increases from 0.78 to 0.81, and G1 has the greatest influence on the power factor of the motor. The change in motor efficiency with C1, G1, and D1 is shown in Figure 8d. With the increase in C1, the motor efficiency decreases continuously, with a decrease of 0.2%. With the increases in G1 and D1, the efficiency of the motor increases first and then decreases, and G1 has the greatest influence on the efficiency of the motor.

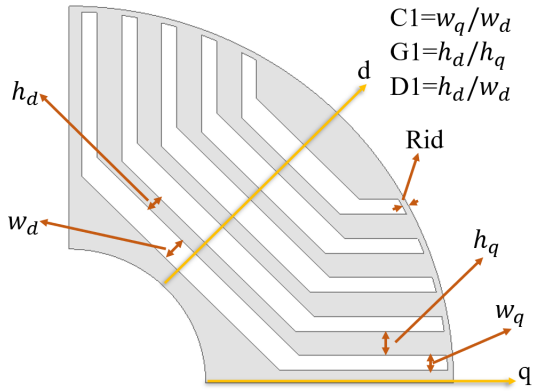

Figure 7. Cross-section of synchronous reluctance motor.

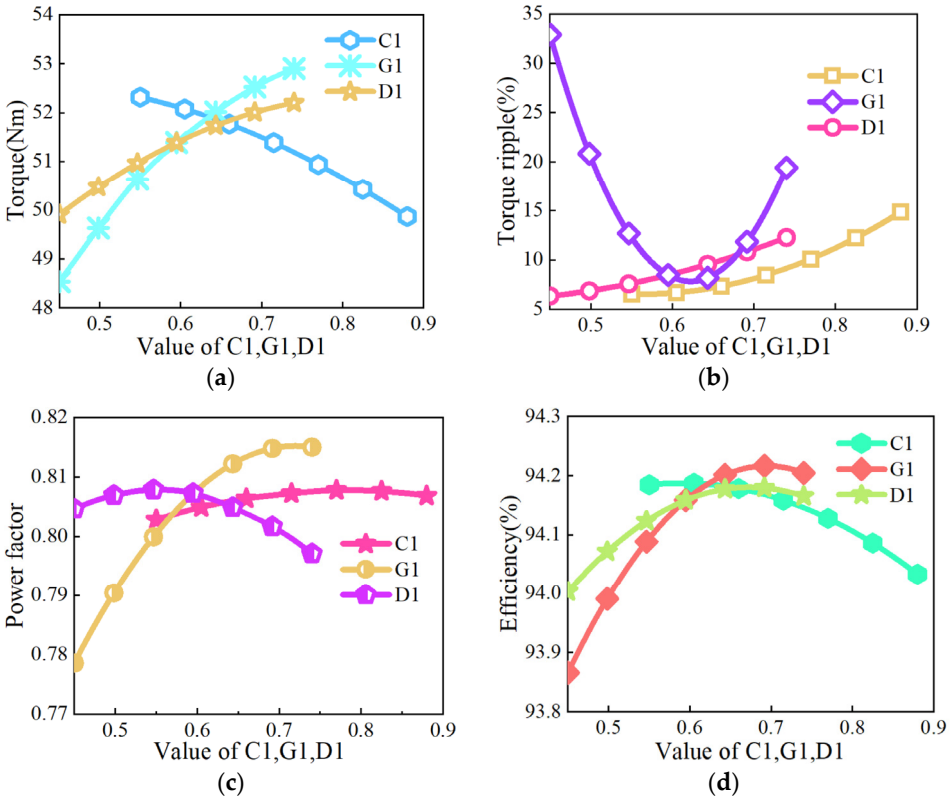

Figure 8. Influence of optimized parameters on motor performance. (**a**) Torque. (**b**) Torque ripple. (**c**) Power factor. (**d**) Efficiency.

According to the above analysis, it can be seen that w_d, C1, G1, and D1 have an impact on the performance of the synchronous reluctance motor, so wd, C1, G1, and D1 are selected as the optimization parameters. In addition, according to the arrangement space of the magnetic barrier on the rotor, the variation range of w_d, C1, G1, and D1 is determined, as shown in Table 4.

Table 4. Optimization parameters of synchronous reluctance motor and its value range.

Symbol	Parameter	Range
w_d (mm)	Thickness of d-axis magnetic barrier	[3.5,5.5]
C1	The ratio of q-axis and d-axis magnetic barrier thickness (w_q/w_d)	[0.55,0.88]
G1	The ratio of the thickness of the d-axis and q-axis magnetic layers (h_d/h_q)	[0.45,0.74]
D1	The ratio of the thickness of the d-axis magnetic layer to the thickness of the d-axis magnetic barrier (h_d/w_d)	[0.45,0.74]

Figure 9 shows the sensitivity of the four optimization parameters to the motor performance. It can be seen that w_d and G1 have the highest sensitivity to the main output performance of the motor, followed by C1 and D1. On the whole, these four parameters need to be optimized in the next step to obtain the optimal value.

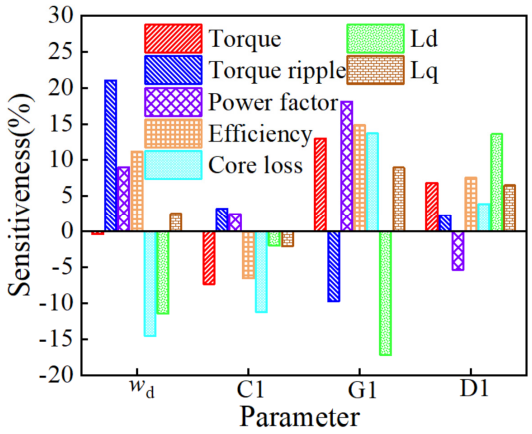

Figure 9. Sensitivity of optimization parameters of synchronous reluctance motor.

The optimization goal of the synchronous reluctance motor is shown in Formula (1), which requires the motor to achieve the highest efficiency and minimum torque ripple.

Efficiency: Efficiency is one of the important performance indicators of the motor. In this paper, the amount of efficiency is calculated as the ratio of the output power of the motor to the input power, which is also a commonly used calculation method for motor efficiency testing.

Torque ripple: The torque ripple of the motor will directly affect the stability of its output torque and the vibration noise. In this paper, the calculation method of motor torque ripple is the ratio of the difference between the maximum and minimum output torque to the average output torque.

$$Objectives: \begin{cases} \max(\eta_1) \\ \min(T_{r1}) \end{cases} \quad (1)$$

where η_1 is the efficiency of synchronous reluctance motor; T_{r1} is the torque ripple of synchronous reluctance motor.

The constraints of synchronous reluctance motor optimization are shown in Equation (2). The motor is required to achieve the rated torque, and the power factor should be greater than 0.8.

Output torque: The output torque is the primary parameter of the motor. When evaluating a motor, it is first necessary to make the motor reach the rated torque, and then look at other performances of the motor.

Power factor: Power factor is also an important performance index to evaluate the motor. For the permanent magnet-assisted synchronous reluctance motor, the power factor

is proportional to the salient pole ratio of the motor rotor, which can reflect the design of the motor.

$$Constrains: \begin{cases} T_1 \geq 47.8Nm \\ \cos\varphi_1 \geq 0.8 \end{cases} \quad (2)$$

where T_1 is the output torque of a synchronous reluctance motor; $\cos\varphi_1$ is the power factor of a synchronous reluctance motor.

The multi-objective genetic algorithm is used to optimize the synchronous reluctance motor, and the optimization results are shown in Table 5.

Table 5. Optimization results of synchronous reluctance motor.

Symbol	Optimal Results
w_d (mm)	4.27
C1	0.625
G1	0.589
D1	0.599

3.3. Multi-Objective Optimization Design of PMA-Synrm

The cross-section of a permanent magnet-assisted synchronous reluctance motor is shown in Figure 10. In the figure, it can be seen that the design parameters of this motor are d-axis magnetic barrier thickness w_d, five-layer ferrite length L1-L5, and circumferential magnetic bridge Rid. Among them, the synchronous reluctance motor is optimized in the previous section, and the optimal values of C1, G1, and D1 are obtained, which are 0.625, 0.589, and 0.599 respectively. Therefore, w_q, h_d, and h_q can be represented by C1, G1, D1, and w_d.

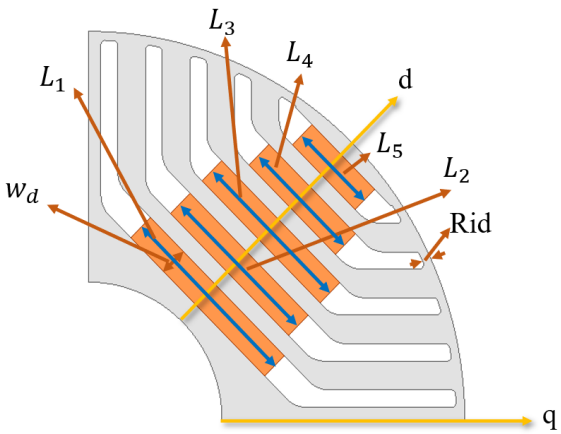

Figure 10. Section diagram of permanent magnet-assisted synchronous reluctance motor.

Table 6 shows the range of these seven optimization parameters. Due to the limited area of the magnetic barrier and ferrite arranged on the rotor, the value range of each parameter can be obtained according to the analysis.

Before the optimization design of the permanent magnet-assisted synchronous reluctance motor, the sensitivity analysis of the main optimized parameters is carried out by means of the finite element model, and the correlation coefficient of each optimization parameter to different optimization objectives is obtained. In this paper, the Pearson correlation coefficient is used to represent the influence of each optimization parameter on different optimization objectives. The specific results are shown in Figure 11.

Table 6. Optimization parameters and range of PMA-Synrm.

Symbol	Parameter	Range
w_d (mm)	Thickness of d-axis magnetic barrier	[3.5,5.5]
Rid	Length of circumferential magnetic bridge	[0.5,2]
L1	Length of the first layer of ferrite	[30,40]
L2	Length of the second layer ferrite	[30,40]
L3	Length of the third layer of ferrite	[25,35]
L4	Length of the fourth layer of ferrite	[20,30]
L5	Length of the fifth layer of ferrite	[15,25]

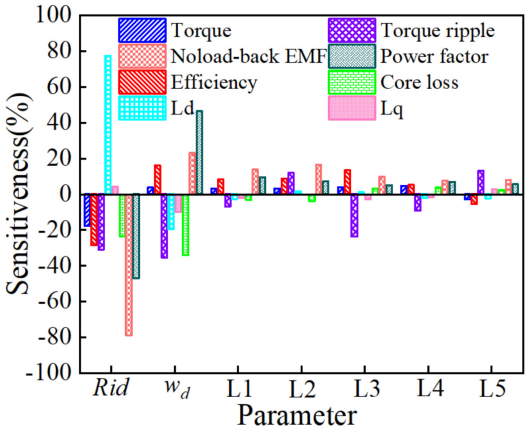

Figure 11. Sensitivity of optimization parameters of PMA-Synrm to motor performance.

Figure 12 shows the response surface fitting curve of the seven design parameters of the permanent magnet-assisted synchronous reluctance motor on the main electromagnetic performance of the motor. Among them, the width of the circumferential magnetic bridge Rid has a great influence on the performance of the motor. The main function of the circumferential magnetic bridge is to prevent magnetic flux leakage, so it needs to be designed emphatically. The increase in the thickness of w_d will increase the salient pole ratio of the motor and improve the performance of the motor, but when it is too large, it will lead to serious magnetic saturation of the motor and reduce the output torque, efficiency, and power factor of the motor, and will increase the torque ripple. L1-L5 is the length of five layers of ferrite. The increase in length means an increase in ferrite content. In a certain range, it can provide a stronger magnetic field to help improve the output torque, efficiency, and other performance of the motor. However, when the increase is too large, it will also lead to serious rotor magnetic saturation, which will increase the iron loss, reduce the efficiency of the motor, reduce the rotor salient ratio, and reduce the power factor of the motor. The influence of L1–L5 on the torque ripple of the motor is different. The increase in L1, L2, and L4 will make the torque ripple decrease first and then increase, and the variation range is 3%, 5%, and 4%, respectively. The increase in L3 and L5 will make the torque ripple decrease continuously, and the change ranges are 11% and 6%, respectively.

The optimization objective of the permanent magnet-assisted synchronous reluctance motor is shown in Equation (3). Similarly, in order to achieve the performance index of the motor, the maximum efficiency of the motor and the minimum output torque ripple are required to ensure the stable operation of the motor.

$$Objectives: \begin{cases} \max(\eta_2) \\ \min(T_{r2}) \end{cases} \tag{3}$$

where η_2 is the efficiency of PMA-Synrm, and T_{r2} is the torque ripple of PMA-Synrm.

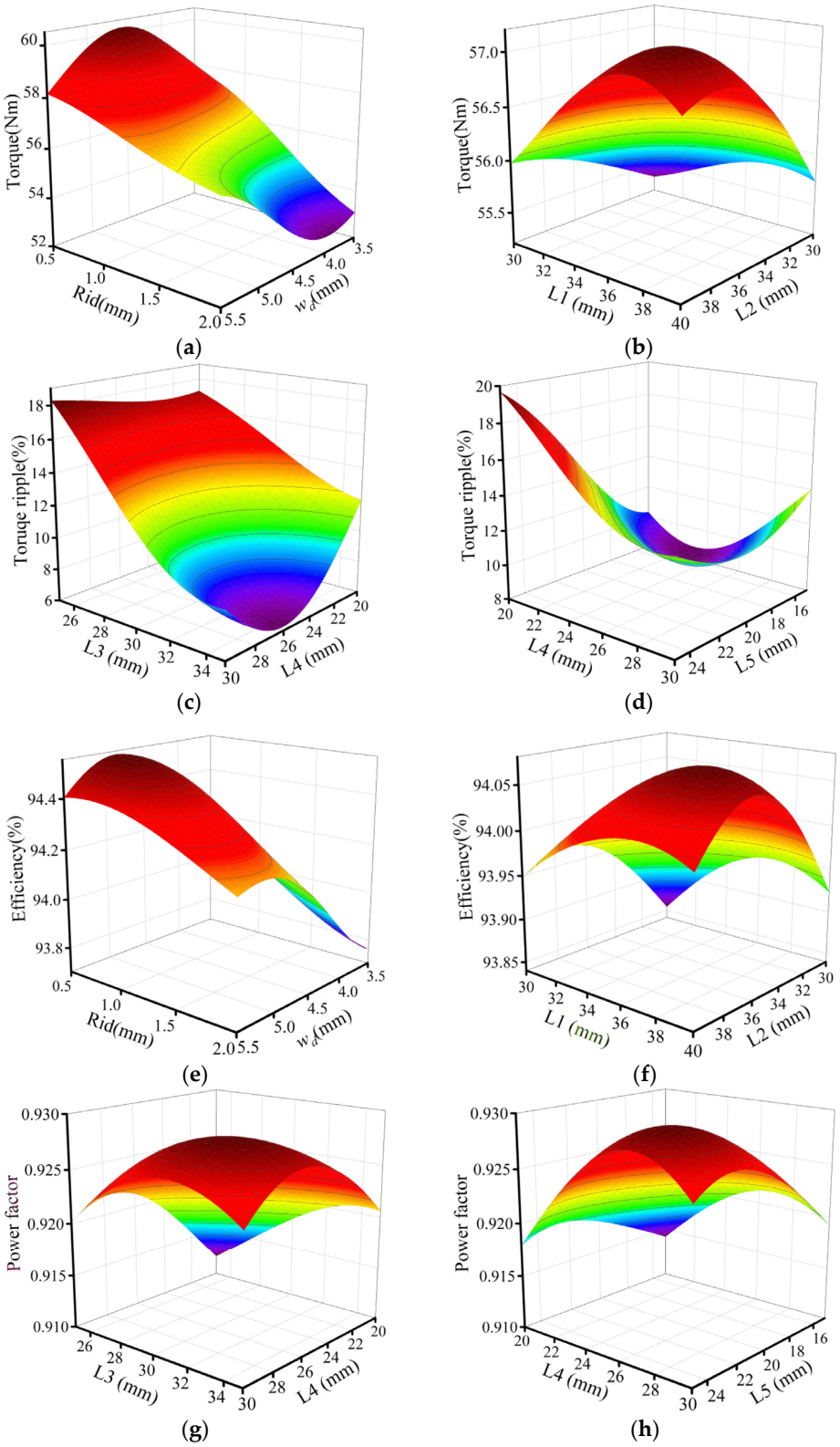

Figure 12. Response surface fitting results of optimized parameters on motor performance. (**a**,**b**) Torque. (**c**,**d**) Torque ripple. (**e**,**f**) Efficiency. (**g**,**h**) Power factor.

According to the performance index required by the motor, the constraint conditions for the optimization of the permanent magnet-assisted synchronous reluctance motor can

be set, as shown in Formula (4). It is necessary to reach the rated torque of the motor, and in order to design the margin, the power factor needs to be higher than 0.91.

$$Constrains: \begin{cases} T_2 \geq 47.8Nm \\ \cos \varphi_2 \geq 0.91 \end{cases} \quad (4)$$

where T_2 is the output torque of PMA-Synrm, and $\cos \varphi_2$ is the power factor of PMA-Synrm.

The Latin hypercube sampling design method (LHS) is used to collect sample points; the Kriging method is used to establish the surrogate model, and the multi-objective genetic algorithm (NSGA-II) is used to optimize the motor. The final optimization results are shown in Table 7.

Table 7. Optimization results of permanent magnet-assisted synchronous reluctance motor.

Symbol	Optimal Results
w_d (mm)	4.70
h_d (mm)	2.82
w_q (mm)	2.94
h_q (mm)	4.78
Rid (mm)	1.0
L1 (mm)	38
L2 (mm)	38
L3 (mm)	34
L4 (mm)	28
L5 (mm)	21.6

3.4. Optimization Results and Finite Element Verification of PMA-Synrm

The magnetic cloud diagram of the motor load before and after the optimization of the permanent magnet-assisted synchronous reluctance motor is shown in Figure 13. It can be seen from the diagram that the magnetic saturation degree of the multi-layer magnetic conductive layer on the rotor of the motor before optimization is high, and there are several stator teeth close to saturation. However, the degree of magnetic saturation on the stator and rotor of the optimized motor is greatly reduced.

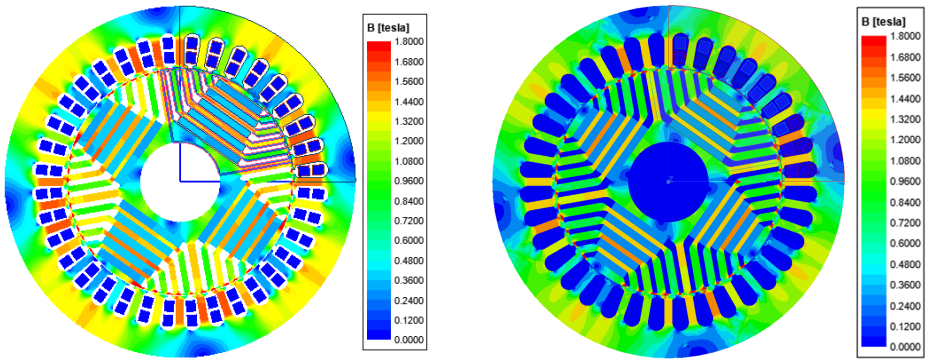

(**a**) initial (**b**) optimal

Figure 13. Magnetic density cloud diagram of motor load before and after optimization. (**a**) Initial. (**b**) Optimal.

Figure 14 shows the no-load back EMF waveform and harmonic distribution before and after optimization of the permanent magnet-assisted synchronous reluctance motor. It can be seen from Figure 14a that the effective value of the no-load back EMF of the motor before optimization is slightly higher than that after optimization, but the no-load back EMF waveform of the optimized motor is more sinusoidal. In addition, the harmonics of

the optimized motor are mainly 15 and 17 times, and the harmonic content is much less than that before optimization, as shown in Figure 14b.

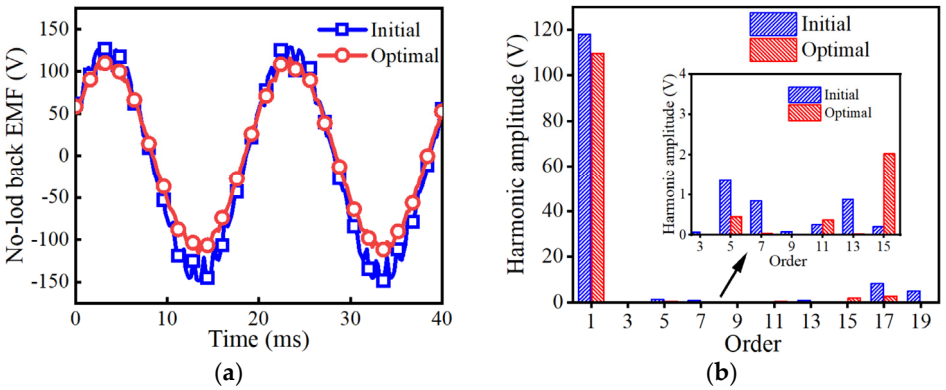

Figure 14. The no-load back-EMF waveform and harmonic distribution of the PMA-Synrm before and after optimization. (**a**) No-load back EMF waveform. (**b**) No-load back EMF harmonic distribution.

Figure 15 shows the no-load radial air gap flux density waveform and harmonic distribution before and after optimization of the permanent magnet-assisted synchronous reluctance motor. It can be seen from Figure 15a that the no-load back EMF of the optimized motor is slightly lower than that before optimization, but the optimized air gap flux density waveform is more sinusoidal. As shown in Figure 15b, the no-load air gap harmonics of the optimized motor are mainly 17 and 19 harmonics, and the harmonic content and the amplitude of the magnetic isolation harmonics are small.

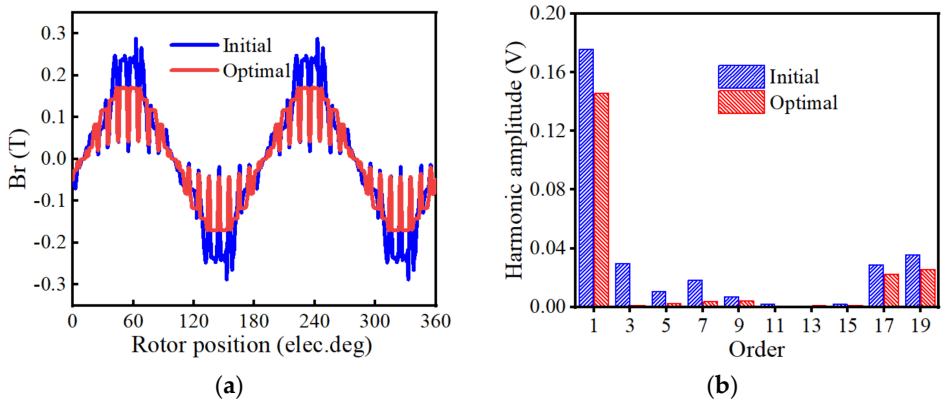

Figure 15. The no-load radial air gap flux density waveform and harmonic distribution of the permanent magnet-assisted synchronous reluctance motor before and after optimization. (**a**) No-load radial air gap flux density waveform. (**b**) No-load radial air gap flux density waveform harmonic distribution.

Figure 16 shows the torque characteristics and electromagnetic performance of the permanent magnet-assisted synchronous reluctance motor before and after optimization. As shown in Figure 16a, the average torque of the optimized motor is 49.7 Nm, which is 0.5 Nm lower than that before optimization. However, the optimized torque ripple is only 4.8%, which is 10.8% lower than that before optimization. It can be seen from Figure 16b that the efficiency of the optimized motor is 94.1%, which is 0.6% higher than that before optimization. Because the optimized no-load back EMF decreases slightly, the optimized power factor is slightly smaller than that before optimization.

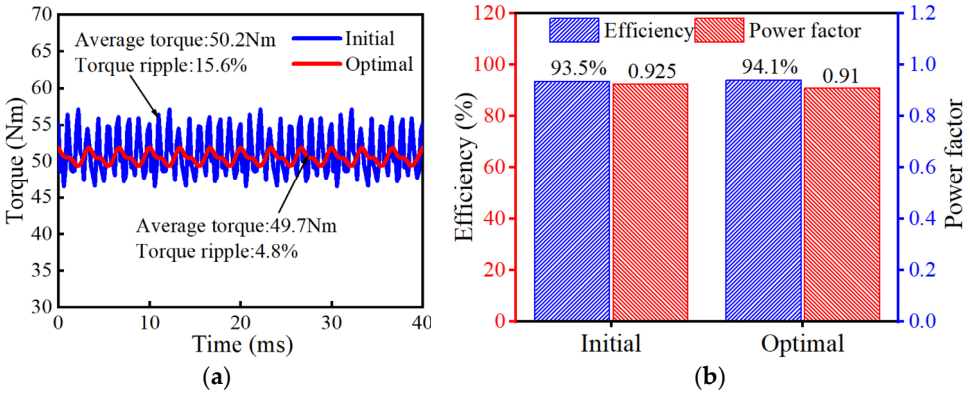

Figure 16. The torque characteristics and electromagnetic performance of the motor before and after optimization. (**a**) Output torque and torque ripple. (**b**) Efficiency and power factor.

The temperature simulation of the motor is carried out by using the thermal module of Motor-CAD. The motor uses the same heat dissipation method as the asynchronous motor; that is, the casing has a heat dissipation fin, the shaft sleeve fan, and the fairing is used to distribute the air volume to take away the heat of the motor. The operating environment temperature of the motor is set to 30 °C. After analysis, it can be seen that the temperature distribution of the motor before and after optimization is shown in Figure 17. The maximum temperature of the optimized motor is only 76.6 °C, which is 2.2 °C lower than that of the initial scheme. After optimization, the iron loss of the motor rotor is reduced, so the core temperature of the optimized motor rotor is lower than the rotor temperature of the initial design scheme.

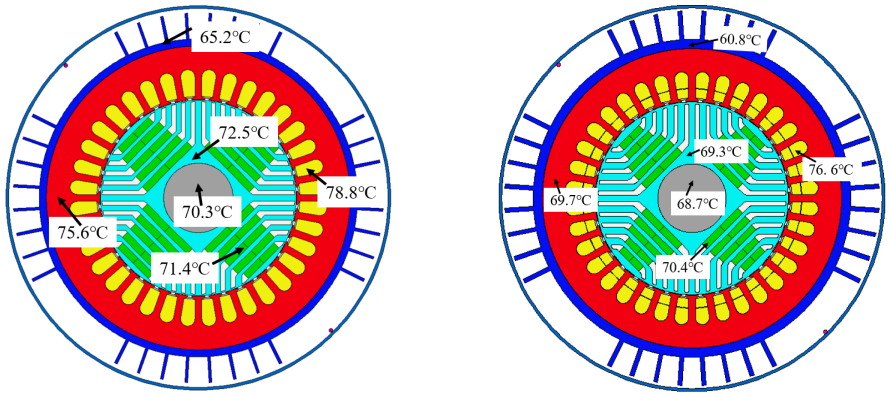

Figure 17. Temperature distribution of permanent magnet-assisted synchronous reluctance motor before and after optimization. (**a**) Initial design of motor temperature. (**b**) Optimized motor temperature.

Table 8 compares the results of optimization prediction with the results of finite element calculation. It can be seen from the table that the difference between the torque ripple is only 0.2%, and the difference between the core loss is the largest, reaching 3.8 W, and the difference between other parameters is small. From the comparison of the two results, it can be seen that the parameter dimension reduction optimization method proposed in this paper is feasible and effective.

Table 8. The optimization results of permanent magnet-assisted synchronous reluctance motor are compared with finite element results.

Parameter Name	Initial Value	Predicted Value	Simulative Value	Error
Current (A)	13.6	13.3	13.4	+0.1
Output torque (Nm)	50.2	50.1	49.7	−0.4
Torque ripple (%)	15.6	4.6	4.8	+0.2
No-load back EMF (V)	85	77.52	77.37	−0.15
Core loss	147.6	130.4	134.2	+3.8
Power factor	0.925	0.914	0.910	−0.004
Efficiency (%)	93.5	94.15	94.1	−0.05

4. Experimental Verification

Based on the above optimization results, a prototype of a 7.5 kW, 1500 rpm permanent magnet-assisted synchronous reluctance motor was fabricated. The prototype structure is shown in Figure 18.

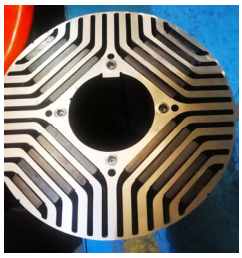

Figure 18. Permanent magnet-assisted synchronous reluctance motor rotor structure diagram.

The prototype is tested experimentally, and the data of no-load and load of the motor are shown in Figure 19. It can be seen from Figure 19a that when the motor is running at the rated load, the measured load current is 13.5 A, and the simulated load current is 13.2 A. Figure 19b shows the curve of no-load back EMF. When the prototype is running at no-load, the measured no-load back EMF is 76.1 V, which is 1.27 V lower than the simulated value. In addition, the optimized prediction value, finite element calculation results, and prototype test results are summarized in Table 9. It can be seen that the three results are not much different. It can be further proved that the parameter dimension reduction optimization method proposed in this paper can ensure the accuracy of the optimization results while reducing the optimization parameters and improving the optimization efficiency.

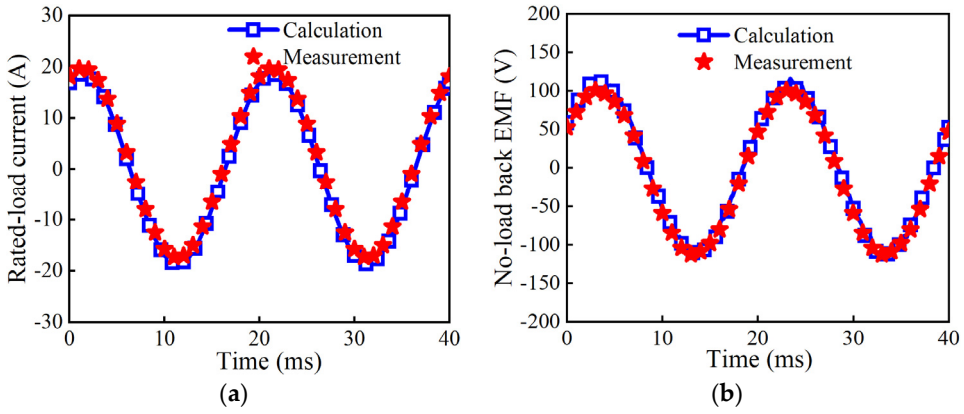

Figure 19. Prototype test data and calculation data curve. (**a**) No-load back EMF curve. (**b**) Rated-load current curve.

Table 9. The optimization results of permanent magnet-assisted synchronous reluctance motor are compared with finite element results.

Parameter	Predicted Value	Simulative Value	Measurement
Output power (kW)	7.50	7.50	7.52
Rated-load current (A)	13.3	13.4	13.5
No-load back EMF (V)	77.52	77.37	76.10
Power factor	0.914	0.910	0.905
Efficiency (%)	94.15	94.10	94.06

5. Conclusions

This paper is based on a 7.5 kW, 1500 rpm permanent magnet-assisted synchronous reluctance motor. The motor rotor is composed of five layers of magnetic barriers and five layers of ferrite. The design parameters of the motor rotor are as high as 26. The multi-objective genetic algorithm is used to optimize the design of the motor. The specific conclusions of this paper and future research work are as follows:

- In this paper, by analyzing the influence of the design parameters of the rotor magnetic barrier on the main output performance of the motor, considering the convenience of the actual processing of the motor, a parameter dimension reduction optimization design method is proposed. Using this method, the optimization parameters of the permanent magnet-assisted synchronous reluctance motor can be reduced from 26 to 7, which greatly improves the optimization efficiency of the permanent magnet-assisted synchronous reluctance motor and realizes the comprehensive global optimization design of the permanent magnet-assisted synchronous reluctance motor. The optimization design method can provide a reference for motor designers to a certain extent;
- At present, the motor is developing in the direction of "no rare earth, light rare earth". The permanent magnet-assisted synchronous reluctance motor, as a motor only assisted by ferrite, is in line with the current development trend. Moreover, the size of the permanent magnet-assisted synchronous reluctance motor in this paper mainly refers to the same power asynchronous motor. After design and optimization, the efficiency and other performance indicators of the permanent magnet-assisted synchronous reluctance motor can fully reach the IE5 energy efficiency level. Therefore, it is necessary to conduct more in-depth research on the permanent magnet-assisted synchronous reluctance motor to achieve higher efficiency.

Author Contributions: Conceptualization, Z.L.; data curation, Z.L. and G.Z.; formal analysis, Z.L. and G.Z.; funding acquisition, Z.L.; investigation, Z.L. and G.Z.; methodology, Z.L. and G.Z.; project administration, Z.L.; resources, Z.L.; software, G.Z.; supervision, G.D.; validation, Z.L., G.Z. and G.D.; visualization, G.Z.; writing—original draft, Z.L.; writing—review and editing, Z.L., G.Z. and G.D. All authors have read and agreed to the published version of the manuscript.

Funding: This research received no external funding.

Institutional Review Board Statement: Not applicable.

Informed Consent Statement: Not applicable.

Data Availability Statement: Data are contained within this article.

Conflicts of Interest: The authors declare no conflicts of interest.

References

1. Morimoto, S.; Ooi, S.; Inoue, Y.; Sanada, M. Experimental Evaluation of a Rare-Earth-Free PMASynRM with Ferrite Magnets for Automotive Applications. *IEEE Trans. Ind. Electron.* **2014**, *61*, 5749–5756. [CrossRef]
2. Guan, Y.; Zhu, Z.Q.; Afinowi, I.A.A.; Mipo, J.C.; Farah, P. Design of Synchronous Reluctance and Permanent Magnet Synchronous Reluctance Machines for Electric Vehicle Application. In Proceedings of the 17th International Conference on Electrical Machines and Systems (ICEMS), Hangzhou, China, 22–25 October 2014. [CrossRef]
3. Zhang, Y.; Yu, S.Y.; Liu, G.W.; Zhang, H. Comparative Research for a Novel Dual-Stator Synchronous Machine with Permanent Magnet-Reluctance Composite Rotor. *IEEE Trans. Appl. Supercond.* **2020**, *30*, 5203505. [CrossRef]
4. Du, G.; Zhang, G.; Li, H.; Hu, C. Comprehensive Comparative Study on Permanent-Magnet-Assisted Synchronous Reluctance Motors and Other Types of Motor. *Appl. Sci.* **2023**, *13*, 8557. [CrossRef]
5. Cai, H.; Guan, B.; Xu, L. Low-Cost Ferrite PM-Assisted Synchronous Reluctance Machine for Electric Vehicles. *IEEE Trans. Ind. Electron.* **2014**, *61*, 5741–5748. [CrossRef]
6. Wang, Y.; Bacco, G.; Bianchi, N. Geometry Analysis and Optimization of PM-Assisted Reluctance Motors. *IEEE Trans. Ind. Appl.* **2017**, *53*, 4338–4347. [CrossRef]
7. Ferrari, M.; Bianchi, N.; Fornasiero, E. Analysis of Rotor Saturation in Synchronous Reluctance and PM-Assisted Reluctance Motors. *IEEE Trans. Ind. Appl.* **2015**, *51*, 169–177. [CrossRef]
8. Ferrari, M.; Bianchi, N.; Fornasiero, E. Rotor Saturation Impact in Synchronous Reluctance and PM Assisted Reluctance Motors. In Proceedings of the 2013 IEEE Energy Conversion Congress and Exposition, Denver, CO, USA, 15–19 September 2013; pp. 1235–1242.
9. Kong, Y.; Lin, M.; Yin, M.; Hao, L. Rotor Structure on Reducing Demagnetization of Magnet and Torque Ripple in a PMa-synRM with Ferrite Permanent Magnet. *IEEE Trans. Magn.* **2018**, *54*, 8108705. [CrossRef]
10. Huang, H.; Hu, Y.-S.; Xiao, Y.; Lyu, H. Research of Parameters and Antidemagnetization of Rare-Earth-Less Permanent Magnet-Assisted Synchronous Reluctance Motor. *IEEE Trans. Magn.* **2015**, *51*, 8112504. [CrossRef]
11. Liu, H.-C.; Kim, I.-G.; Oh, Y.J.; Lee, J.; Go, S.-C. Design of Permanent Magnet-Assisted Synchronous Reluctance Motor for Maximized Back-EMF and Torque Ripple Reduction. *IEEE Trans. Magn.* **2017**, *53*, 8202604. [CrossRef]
12. Huynh, T.A.; Hsieh, M.-F.; Shih, K.-J.; Kuo, H.-F. An Investigation Into the Effect of PM Arrangements on PMa-SynRM Performance. *IEEE Trans. Ind. Appl.* **2018**, *54*, 5856–5868. [CrossRef]
13. Ji, Z.; Li, H.; Chen, Z.; Yu, T.; Liu, L.; Ma, M. Design and optimization of permanent magnet assisted synchronous reluctance motor for better torque performance. In Proceedings of the 2019 22nd International Conference on Electrical Machines and Systems (ICEMS), Harbin, China, 11–14 August 2019; pp. 1–4.
14. Xie, Y.; Yang, F.; Wang, L. Novel PM-Assisted Synchronous Reluctance Machines Using Asymmetrical Rotor Configuration. *IEEE Access* **2022**, *10*, 79564–79573. [CrossRef]
15. Xu, M.M.; Liu, G.H.; Chen, Q. Fast calculation method of optimal flux-barrier-end position for torque ripple minimisation in SynRMs with and without PMs. *IET Electr. Power Appl.* **2020**, *14*, 705–715. [CrossRef]
16. López, C.; Sala, E.; Espinosa, A.; Romeral, L. Constrained-Size Torque Maximization in SynRM Machines by Means of Genetic Algorithms. In Proceedings of the IEEE 10th International Symposium on Diagnostics for Electrical Machines, Power Electronics and Drives (SDEMPED 2015), Guarda, Portugal, 1–4 September 2015. [CrossRef]
17. Diao, K.; Sun, X.; Lei, G.; Guo, Y.; Zhu, J. Multiobjective System Level Optimization Method for Switched Reluctance Motor Drive Systems Using Finite-Element Model. *IEEE Trans. Ind. Electron.* **2020**, *67*, 10055–10064. [CrossRef]
18. Degano, M.; Murataliyev, M.; Shuo, W.; Barater, D.; Buticchi, G.; Jara, W.; Bianchi, N.; Galea, M.; Gerada, C. Optimised Design of Permanent Magnet Assisted Synchronous Reluctance Machines for Household Appliances. *IEEE Trans. Energy Convers.* **2021**, *36*, 3084–3095. [CrossRef]
19. Kim, H.; Park, Y.; Oh, S.-T.; Jang, H.; Won, S.-H.; Chun, Y.-D.; Lee, J. A Study on the Rotor Design of Line Start Synchronous Reluctance Motor for IE4 Efficiency and Improving Power Factor. *Energies* **2020**, *13*, 5774. [CrossRef]
20. Kim, H.; Park, Y.; Oh, S.-T.; Jeong, G.; Seo, U.-J.; Won, S.-H.; Lee, J. Study on Analysis and Design of Line-Start Synchronous Reluctance Motor Considering Rotor Slot Opening and Bridges. *IEEE Trans. Magn.* **2022**, *58*, 8103906. [CrossRef]
21. Xu, G.; Jia, Z.; Chen, Q.; Xia, J.; Cai, Y.; Zhang, Z. A Fast and Effective Optimization Procedure for the Ferrite PMaSynRM to Reduce Material Cost. *IEEE Trans. Transp. Electrific.* **2024**, *10*, 635–647. [CrossRef]
22. Hua, Y.; Zhu, H.; Gao, M.; Ji, Z. Multiobjective Optimization Design of Permanent Magnet Assisted Bearingless Synchronous Reluctance Motor Using NSGA-II. *IEEE Trans. Ind. Electron.* **2021**, *68*, 10477–10487. [CrossRef]